



**HAL**  
open science

## Design of model tokamak particles for future toxicity studies: Morphology and physical characterization

E. Bernard, F. Jambon, I. Georges, M. Sanles Sobrido, Jérôme Rose, N. Herlin-Boime, F. Miserque, P. Beaunier, D. Vrel, S. Dine, et al.

### ► To cite this version:

E. Bernard, F. Jambon, I. Georges, M. Sanles Sobrido, Jérôme Rose, et al.. Design of model tokamak particles for future toxicity studies: Morphology and physical characterization. Fusion Engineering and Design, 2019, 145, pp.60-65. 10.1016/j.fusengdes.2019.05.037 . hal-02169319

**HAL Id: hal-02169319**

**<https://hal.science/hal-02169319>**

Submitted on 8 Jul 2019

**HAL** is a multi-disciplinary open access archive for the deposit and dissemination of scientific research documents, whether they are published or not. The documents may come from teaching and research institutions in France or abroad, or from public or private research centers.

L'archive ouverte pluridisciplinaire **HAL**, est destinée au dépôt et à la diffusion de documents scientifiques de niveau recherche, publiés ou non, émanant des établissements d'enseignement et de recherche français ou étrangers, des laboratoires publics ou privés.

# Design of model tokamak particles for future toxicity studies: morphology and physical characterization

*E. Bernard<sup>1</sup>, F. Jambon<sup>2</sup>, I. Georges<sup>2</sup>, M. Sanles Sobrido<sup>3</sup>, J. Rose<sup>3</sup>, N. Herlin-Boime<sup>4</sup>, F. Miserque<sup>5</sup>,  
P. Beaunier<sup>6</sup>, D. Vrel<sup>7</sup>, S. Dine<sup>7</sup>, E. Hodille<sup>1</sup>, J. Chêne<sup>2</sup>, S. Garcia-Argote<sup>2</sup>, G. Pieters<sup>2</sup>, S. Peillon<sup>9</sup>,  
F. Gensdarmes<sup>9</sup>, G. Dinescu<sup>10</sup>, T. Acsente<sup>10</sup>, C. Uboldi<sup>11</sup>, T. Orsiere<sup>11</sup>, V. Malard<sup>8</sup>, B. Rousseau<sup>2</sup>, Ph. Delaporte<sup>12</sup>  
and C. Grisolia<sup>1,13,\*</sup>*

<sup>1</sup>*CEA, IRFM, F-13108 Saint Paul lez Durance, France*

<sup>2</sup>*CEA, SCBM, Université Paris Saclay, F-91191, Gif-sur-Yvette, France*

<sup>3</sup>*Aix Marseille Univ., CNRS, IRD, Collège de France, INRA, CEREGE UMR34, Aix en Provence, France*

<sup>4</sup>*CEA, IRAMIS UMR NIMBE, Université Paris Saclay, 91191 Gif-sur-Yvette, France*

<sup>5</sup>*DEN- Service de la Corrosion et du Comportement des Matériaux dans leur Environnement (SCCME), CEA,  
Université Paris-Saclay, F-91191, Gif-sur-Yvette, France*

<sup>6</sup>*Sorbonne Université, CNRS, Laboratoire de Réactivité de Surface, LRS, 4 place Jussieu, F-75005 Paris,  
France*

<sup>7</sup>*LSPM, Sorbonne Paris Cité, Université Paris 13, UPR 3407 CNRS, 93430 Villetaneuse, France*

<sup>8</sup>*CEA, BIAM, F-13108 Saint Paul lez Durance, France*

<sup>9</sup>*IRSN, PSN-RES/SCA, BP68, 91192 Gif-sur-Yvette, France*

<sup>10</sup>*INFLPR, 409 Atomistilor Street, 77125 Magurele, Bucharest, Romania*

<sup>11</sup>*Aix Marseille Univ, Avignon Université, CNRS, IRD, IMBE, Marseille, France*

<sup>12</sup>*Aix-Marseille Université/CNRS, Laboratoire LP3 (UMR 7341), F-13288 Marseille, France*

<sup>13</sup>*National Research Nuclear University “MEPhI”, Moscow, 115409 Russian Federation*

*Corresponding author: E. Bernard, [elodie.bernard@cea.fr](mailto:elodie.bernard@cea.fr)*

## **Abstract**

During ITER operation, it is expected that the large panel of plasma-wall interactions triggers the production of dust particles, potentially loaded with tritium present nearby. Tritium (T) inventory in the various materials, such as tungsten (W), is of prime importance for the safety assessment of a Tokamak machine, and it is even more crucial when considering dispersible matters like dusts: in case of a Loss Of Vacuum Accident (LOVA), dusts may form aerosols containing tritium and activation products that could escape the first confinement barrier and be released in the environment. The impact of accidental inhalation of such particles has therefore to be evaluated to define appropriate mitigation strategies for fusion workers and the neighboring population. Yet, particles properties in terms of tritium inventory and general behavior are strongly dependent on their physical and chemical characteristics, and until ITER operation starts large uncertainties remain on those parameters; collecting dust produced in existing Tokamaks can give some perspective on possible dust characteristics, but due to the order of magnitude size difference with ITER operation conditions, too little samples can be gathered to lead behavior and toxicity studies. Consequently, a first major step, presented in this paper, is to obtain and characterize potentially relevant W dust samples for toxicity studies. We produced model tungsten (W) Nano-Particles (NPs) by two different methods with characteristics closer to the plasma-wall interaction processes (like ELMs) than grinding (usually used to produce commercial NPs): (i) magnetron plasma sputtering followed by gas condensation as well as (ii) laser ablation. The two types of tungsten NPs obtained exhibit very different properties investigated by a large characterization techniques panel; but both sets show similarities with samples collected in tokamak or observed in dusty plasmas setups, therefore could potentially be expected in ITER. Producing samples with strong differences is an asset to lead a first global study, highlighting which parameters are key, whether it affects the tritium inventory or the toxicity for lung cells during *in vitro* studies. In a second phase, it will help precise the impact of ITER particles when their definition will clarify. The aim of this paper is therefore to study and describe the characteristics of different types of W dusts, this knowledge being mandatory for the next steps of the project dealing

with tritium inventory in the described W dusts and their suspension in various liquid media for cell exposure for toxicity studies.

**Keywords:** tungsten nano-particles, dust, tungsten oxide, fusion technology

## 1. Introduction

Expected power and plasma duration of future fusion devices, such as ITER, requires the plasma-facing components (PFC) to withstand considerable plasma fluxes, in particular the divertor target plates. In this area, tungsten has been chosen for its good resistance to high temperature and its low plasma sputtering yield [1]. However, experiments have shown that the combination of different phenomena (e.g. melting of edges of PFC, material fatigue, intense particle fluxes, material erosion followed by accretion in the plasma edge, ...), particularly during off normal events such as Edge Localized Modes (ELMs) or disruptions, can trigger the formation in the plasma chamber of particles with variable size, ranging from tens of nanometers to hundreds of micrometers [2, 3, 4, 5]. Due to expected much higher energy outflows in ITER compared to the currently operating tokamaks, larger quantities of dust could be produced. Besides, impurities in the Scrape-Off Layer (SOL), such as oxygen, metals and especially gas radiators are expected to enhance physical sputtering of the first wall materials. Particles hence generated will be tritiated as formed in a T environment. Limits have been set by the French Nuclear Safety Authority (ASN) for the inventory of tritium in the vessel (for which dust particles can contribute), but also for the quantity of dust to avoid explosive hazards. This is why although dust production may not be a significant problem in present tokamaks, it is of a major importance to prepare a safe ITER operation by investigating which particles could be produced in this new scale machine, and how they will store tritium. In case of a Loss Of Vacuum Accident (LOVA), particles could be released, causing accidental inhalation for ITER workers: harmful consequences will depend on the

dust physicochemical characteristics and the inhaled dose, it is therefore of major importance to evaluate their potential biological toxicity.

The Passiv-ITER projects fits on that frame: understand and characterize the interaction of tokamak-relevant dust with tritium, with the final outcome of studying the biological impacts of tritiated tungsten nanoparticles (W-NPs) on human lung cells. In ITER, two materials are expected to compose the dust produced during operation: tungsten (W) and beryllium (Be) [6]. Due to safety restrictions on the use of Be particles, we focused our study on W dust. The present work presents a necessary first step, i.e. a detailed description of the dusts characteristics, in order to understand later on their interaction with tritium (which experimental results will be presented separately) and biological systems. Our work has been focused on particles of diameters ranging from 100 to 200 nm. Indeed, High Efficiency Particulate Air (HEPA) filters used to prevent release of particles out of the vacuum chamber present a minimum of efficiency for these particle sizes [7, 8, 9], so they are the most difficult to confine. Moreover, in a toxicity study perspective, larger particles are less likely to be able to permeate cell membranes and therefore have genotoxicity or cytotoxicity effects. Two methods were chosen for their similarity with expected dust-production mechanisms in tokamaks: magnetron plasma sputtering of a W cathode followed by gas condensation, and picosecond laser ablation on a W target. Those two techniques are expected to produce particles of adequate sizes and homogeneous characteristics, whereas mechanical procedures such as grinding used for commercial dust usually do not.

## **2. Discussion on dust production methods and characterization protocols**

As long as ITER is not operating, large uncertainties remain on the morphology, characteristics and size of W NPs that will be produced in this tokamak. Studies on the W PFCs ASDEX Upgrade (AUG) tokamak [10, 11] collected a distribution of particles with

different sizes: flaky particles of 800 nm and spherical ones of 2  $\mu\text{m}$  diameters (with similar size distributions observed through various collection methods), highlighting coexistence of very different morphologies. In the future ITER operation, the plasma characteristics will greatly differ from current tokamaks: operation is expected at very low plasma temperature and high ions density (to reduce as much as possible the conducted power on the divertor target), with longer plasma duration and injection of a radiator such as argon (to enhance the sputtering of the material). In that case, the dusty plasma laboratory conditions could be at play, leading to the creation by accretion of very small particles: their expected size is much smaller than those currently collected in W tokamaks, with dimensions ranging from 10s to 100s of nm [12]. Similarly, multigenerational formation of 30-70 nm diameter particles was also observed through the sputtering of a tungsten samples by hydrogen plasma [13]. This creation process triggers a complex surface morphology, with particles with high Specific Surface Area (SSA) and therefore high surface reactivity. Added to the fact that due to their small size, they might escape HEPA filters and be released, such particles appear as key to consider when evaluating both tritium inventory and toxicity impact.

With the additional constraint to produce samples in sufficient amounts for conclusive biology studies, we chose two dust production methods to generate potentially-relevant ITER-like W particles: magnetron sputtering and gas aggregation (plasma method) [14] and laser ablation (laser method) [15]. In the following part, the dust production techniques are presented as well as the detailed characterization of the physicochemical properties of the particles obtained.

Dust characterization was obtained thanks to the unique coupling of various experimental techniques. First, morphology of the particles was addressed by microscopy observation, using Scanning Electron Microscopy (SEM) and Transmission Electron Microscopy (TEM). For this latter technique, dry samples were suspended in ethanol and deposited on an

observation grid for NPs observation on a JEOL JEM 2010-UHR operating at 200 kV. Image analysis allowed an observation of the shape and size of NPs for each batch; Fourier Transform analysis allowed identification of the crystalline structure. However, in spite of careful grid preparations, the samples nature makes it difficult to use TEM results for quantitative size distribution; we used these results as a qualitative and visual support, as the other techniques at our disposal confirmed the tendencies observed by TEM.

The crystalline state of the W NPs is measured by X-ray Diffraction (XRD) using an INEL Equinox-1000 diffractometer using Cu-K $\alpha$ 1 radiation. X-ray Photoelectron Spectroscopy (XPS) was carried out with a ThermoFisher ESCALAB 250 xi to measure quantitatively the chemical species (*e.g.* W oxidation states) formed on both samples. The proportions of metallic and oxidized tungsten forms were also addressed using X-ray Absorption Spectroscopy (XAS) performed at the European Synchrotron Radiation Facility (Grenoble France) at the W LIII edge. Density of each batch was determined with a Helium Pycnometer Accupyc 1330. Lastly, the Specific Surface Area (SSA) was evaluated using the BET (Brunauer–Emmett–Teller) theory of physical adsorption of gas molecules on a solid surface [16]. Measurements were performed by nitrogen adsorption using a BET COULTER SA3100 instrument. Prior to the measurement, sample outgassing was performed at 150°C during 90 min under nitrogen or helium gas flow. SSA is of importance as mass to surface exposed ratio is a crucial parameter for interactions of the W samples with tritium during the gas loading phase.

### **3. Plasma-produced tungsten nano-particles (Wp NPs)**

#### **3.1. Production**

Wp NPs are produced in a cluster source, where the tungsten vapors produced from W cathode sputtering by a radiofrequency (13.56 MHz) magnetron discharge are condensed in

an argon gas flow; this method is presented in details in [14]. The cluster source is coupled through a nozzle to a deposition chamber continuously pumped down by a turbomolecular pump. The metallic clusters are transported across the nozzle by the gas flow and collected on a substrate at the rate of approximately 5 mg/h.

### 3.2. Physicochemical characterization

#### 3.2.1. Sample morphology and size

Particles produced by magnetron sputtering combined with gas aggregation present a very homogenous size distribution in the diameter range of 100-150 nm (see Fig.1A). This homogeneity is very interesting in the perspective of biology experiments, as size is a crucial parameter for tissue, cell and nucleus barrier passing.

They present different shapes as seen by TEM observation (star-like structures, round or square nano-particles – see Fig. 1B) but all exhibit the same contrast, i.e. similar electron absorption possibly indicating a rather homogenous sample batch.

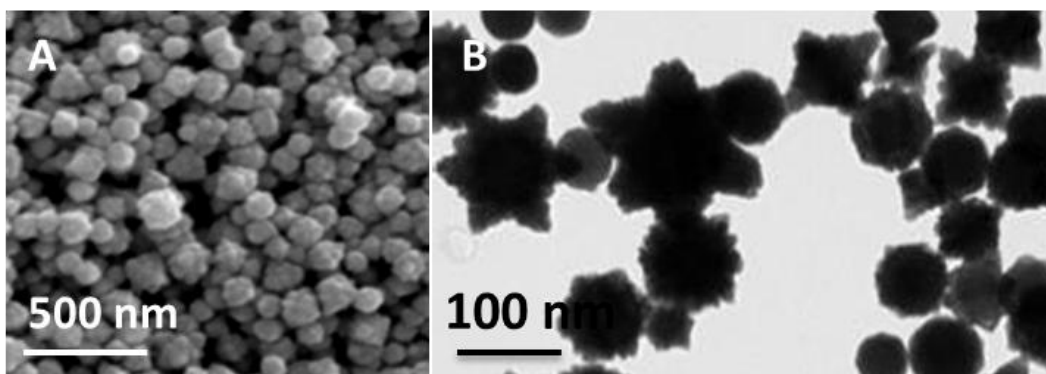


*Fig.1: Plasma-produced NPs observed by SEM present a very high homogeneity in size (A) but with different shapes by TEM observation (B).*

#### 3.2.2. Material properties

High-resolution TEM images show that all Wp NPs are of similar nature: the centre of particles is generally too dense to be analysed, but thinner areas on the rim exhibit clear



crystalline structures (Fig. 2.A and B). Fast Fourier Transform (FFT) patterns are indexed along  $\beta$  phase W metal (Fig. 2.C).

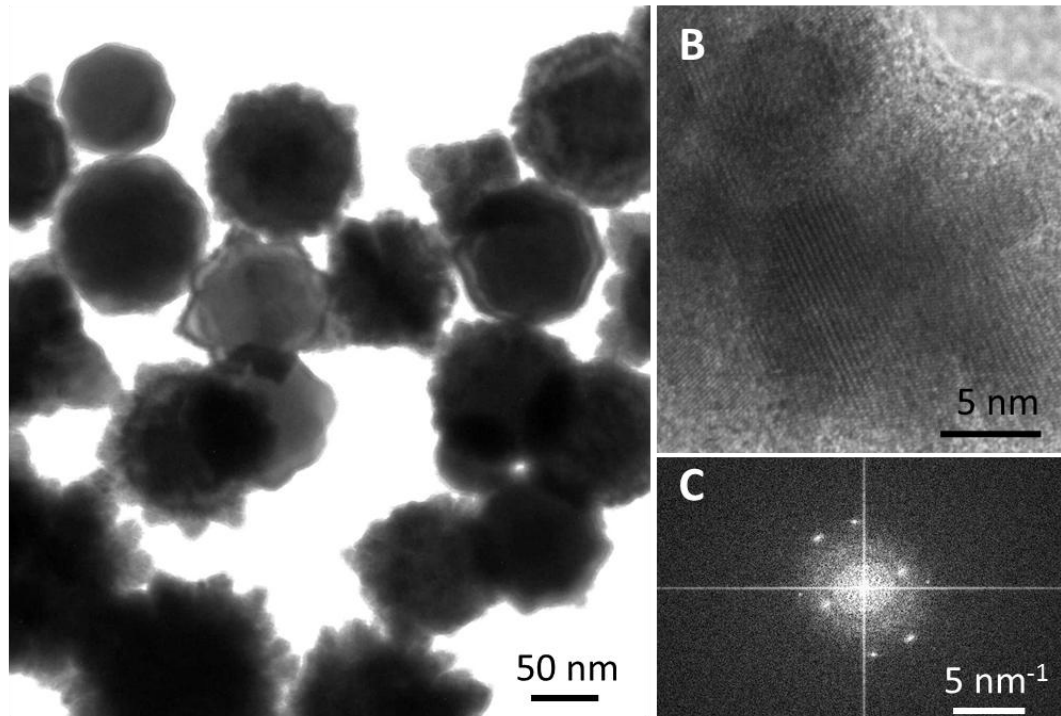


*Fig. 2: High resolution TEM images show the various shapes of Wp NPs (A), with the presence of crystalline planes (B). FFT is consistent with the presence of W metal with (011) orientation in its  $\beta$  phase (C).*

A more macroscopic and statistically relevant approach through XRD was used to characterize the crystal structure of the particles (Fig. 3). The diffraction pattern has been analyzed using Rietveld refinement with the MAUD (Materials Analysis Using Diffraction) software, and confirms the crystalline form of W metal to be almost exclusively the  $\beta$  phase.

The crystal structure of this rare metastable phase of tungsten is present in the inserts of Fig. 3. Due to this specific crystal structure, properties of this material may be significantly different than those of the most common W- $\alpha$ . It is known that the W- $\beta$  phase presents the peculiarity of providing trapping sites for oxygen within its crystal structure [17], so other properties, such as dissolution kinetics, tritium trapping, toxicity... may also be strongly affected.

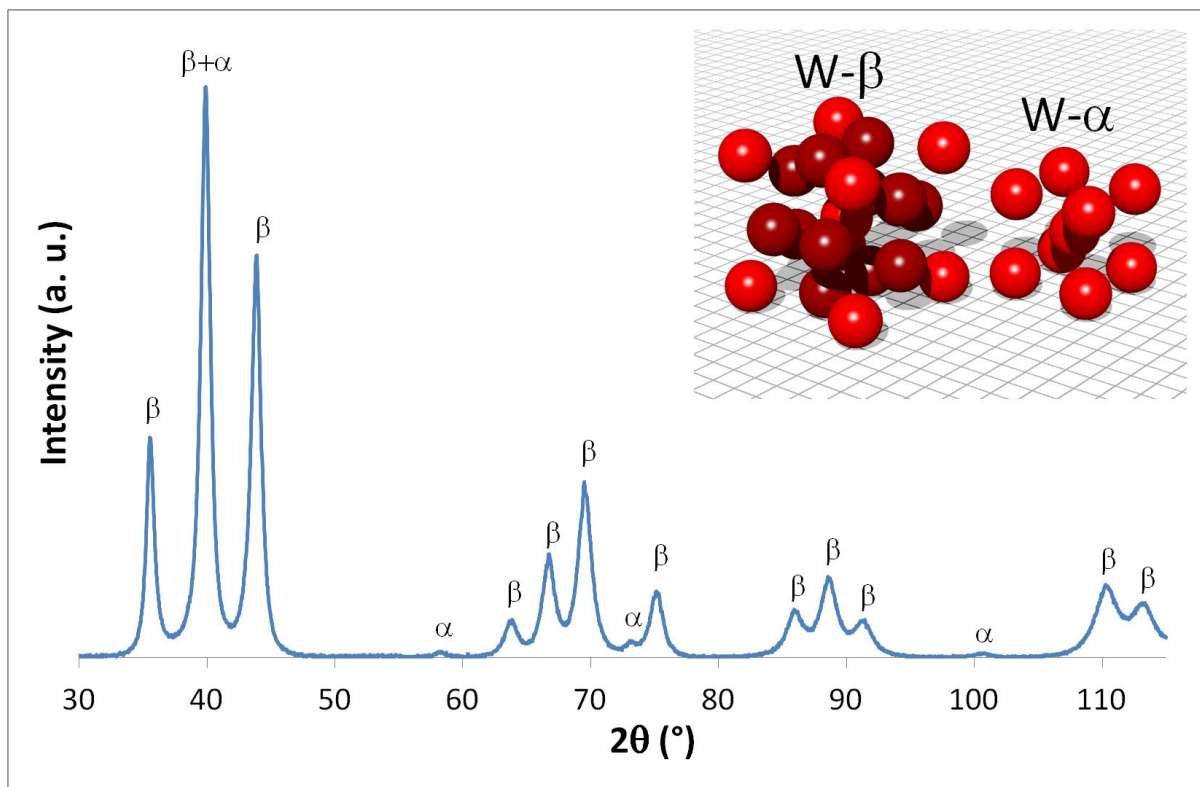


Fig.3: XRD pattern of the Wp NPs, showing a highly dominant W- $\beta$  crystal structure.

Inset: the crystal structures of W- $\alpha$  and W- $\beta$ , with a grid size of 1Å.

Specific Surface Area (SSA) was measured by BET at  $4 \text{ m}^2/\text{g}$ , *i.e.* a value close to the simple geometric calculation of the SSA for a batch of dense spherical particles of diameter 125 nm (SSA of  $3.35 \text{ m}^2/\text{g}$ ): no fractal structure is therefore present and there should not be additional surface reactivity due to internal porosity.

Density measured by helium pycnometer was  $14.32 \text{ g}\cdot\text{cm}^{-3}$ . If we consider the reference densities for W- $\beta$  phase and  $\text{WO}_3$  (respectively  $18.597$  and  $7.16 \text{ g}\cdot\text{cm}^{-3}$ ), we can estimate that W NPs produced by plasma are composed in volume of 62 % W metal and 37 %  $\text{WO}_3$ , or 81.3 wt.% of W and 18.6 wt.%  $\text{WO}_3$ . This composition is consistent with a population of W particles of a 125 nm mean diameter surrounded with a 9 nm native oxide layer at the surface;

such  $\text{WO}_3$  layer is to be expected due to the sample exposure to air between production and characterization.

XAS at the W LIII edge was performed to estimate the proportion of metallic and oxidized form (Fig.4) both near the edge (X-ray Absorption Near Edge Structure (XANES) – see Fig.4.A) and in the fine structure energy zone (Extended X-ray Absorption Fine Structure (EXAFS) – see Fig.4.B) of the sample. Linear combination fitting of the Wp sample (Fig. 4.A, black solid curve at the top captioned “W\_plasma”) indicated that the solid atomic proportion of metal W is  $90\pm 15\%$  (see Fig. 4.A, red dashed curve),  $\text{WO}_3$  representing  $10\pm 15\%$  (see Fig. 4.A, red dashed curve). The conversion to mass leads to  $85\pm 15\%$  W metal. Even if XAS quantitative analysis is known for a lack of precision (uncertainty reaches up to 15% [18]), both XAS and calculation based on density measurements lead to similar estimate of the W/ $\text{WO}_3$  proportion in the W plasma particles.

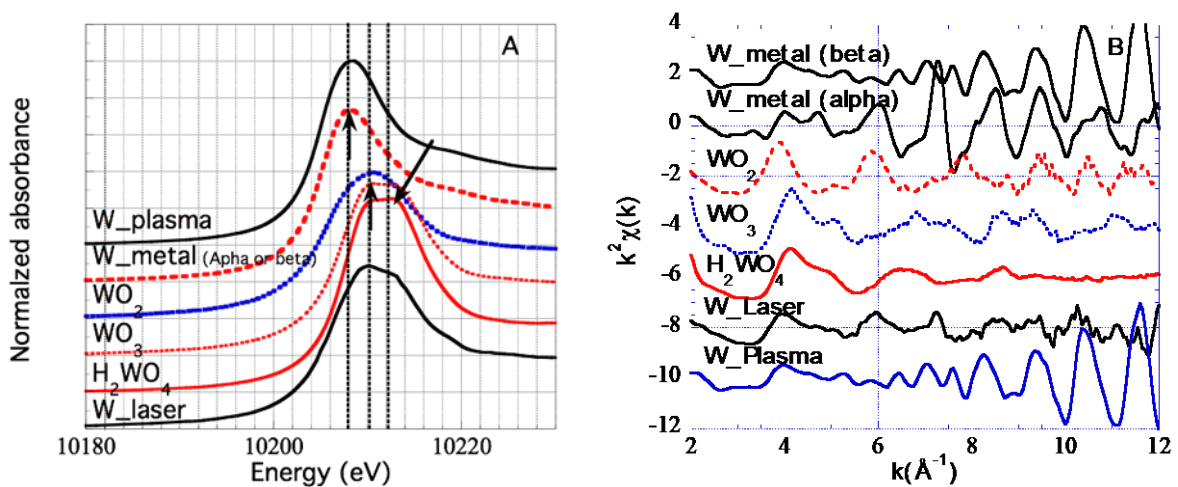


Fig. 4: XANES (A) and EXAFS (B) spectra compared to Wp and Wl samples.

#### 4. Laser-ablation tungsten nano-particles (Wl NPs)

##### 4.1. Production

Preliminary studies [15] highlighted that deposition on material surface using laser with high energy density is an efficient method for creating dust from an initial bulk material with

relative simplicity and flexibility. In metals, absorption of the laser energy triggers the excitation of free electrons, hence increasing their kinetic energy, which is relaxed in the matrix through a thermal wave conveyed by phonons. The laser pulse creates a very short and intense heat source at the material surface, which induces first the generation of a plasma expanding perpendicularly to the surface and second the formation of a thin melted layer in the irradiated area. Then, tungsten particles are formed by accretion of atoms and clusters in the created plasma, and liquid W droplets are ejected from the melted layer because of the pressure applied by the plasma. We used a picosecond laser of wavelength 1064 nm, frequency 10 Hz, pulse energy density  $5 \text{ J/cm}^2$  and pulse duration 50 ps to produce the W NPs. A massive ITER-grade W sample is placed perpendicularly to the laser beam, in a high vacuum chamber with turbomolecular pumping, filled with helium at a pressure of 5000 Pa; the dust production rate is rather low ( $3.5 \text{ mg}\cdot\text{h}^{-1}$ ) but sufficient for our needs. More details about the setup are presented in [19]. The dust produced during the ablation process is gathered by mechanical collection on all surfaces of the ablation chamber.

## **4.2. Physicochemical characterization**

### **4.2.1. Sample morphology and distribution**

TEM observations show that a heterogeneous mix of W dust is produced and collected (Fig.5), where two populations of particles are distinguished.

First, we observe massive crystalline droplets, ejected from the melted tungsten layer at the surface of the ablated massive tungsten sample (see Fig.5.A). These particles are spherical, with diameters ranging from a few tens of nanometers to a few micrometers. Their density is high (no transmission data is available except on the very border of those particles where the material is thin enough for the TEM go through). The production parameters were adjusted in order to limit as much as possible the presence of this type of particles, of reduced interest for

our study. Nevertheless, they are an unavoidable component of the NPs produced by laser ablation in the present configuration.

The second and most important population of WI NPs batch is composed of aggregated particles with a very low contrast on the TEM image, appearing as “foam” (Fig.5.B). They have a diameter of 60-80 nm and this population represents the majority of the collected nanoparticle volume. Some of the structures observed with lighter contrast are of larger size and with spherical shapes (but irregular, contrary to the massive droplets, and do not share their other characteristics).

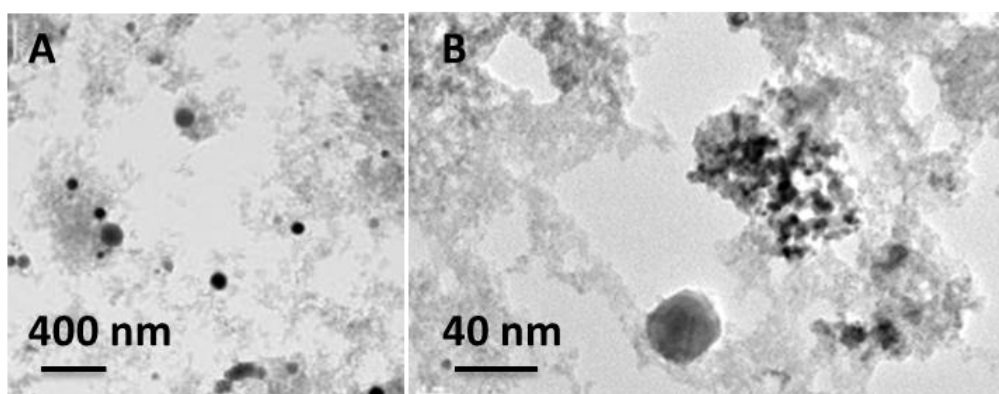


*Fig. 5: Laser-ablation NPs observed by TEM present two distinct populations: high-contrast massive droplet particles with various sizes (A) and aggregated particles mostly amorphous and completely oxidized (B).*

#### **4.2.2. Material properties**

HRTEM images of WI NPs (Fig.6) are more complex to analyse than those obtained for Wp NPs, due to the smaller size of elementary particles and a more diverse particle population. It is difficult to distinguish the material structure in the aggregated and dense areas (Fig.6.A); thinner parts exhibit a mix of amorphous material and small crystallites less than 20 nm long (Fig.6.B). FFT showed that massive droplets rims present a  $\text{WO}_3$  crystalline structure (the centre being too dense to analyse), while aggregated particles are mostly amorphous. Nevertheless, some crystalline structures can be found among aggregated particles, presenting  $\text{WO}_3$  diffraction patterns (Fig.6. C).

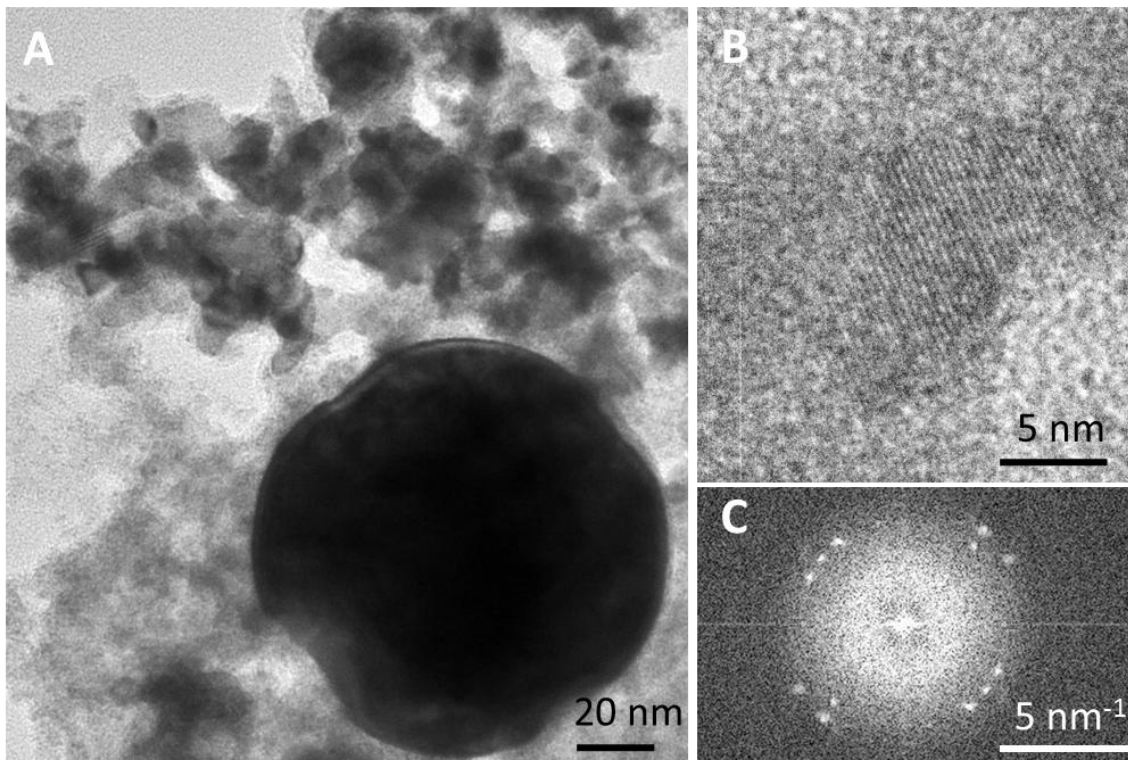


*Fig. 6: High resolution TEM images show the heterogeneous composition of the W1 NPs batch (A), with some crystalline structures appearing (B) in a mostly amorphous particle aggregation. The FFT is consistent with the presence of  $WO_3$  oxide crystallites in the aggregated particle population (C).*

Many areas being too dense for the HRTEM measurement to identify their crystalline structure, we needed a complementary analysis to determine whether the absence of measured W metal lattice planes meant the complete absence of W metallic phase or its absence only in measureable areas. XRD analysis brings the answer: the XRD pattern of the W1 NPs batch (Fig.7) displays the characteristics of the most common crystallographic phase of metallic W, the  $\alpha$  phase (for instance, the one present for W milled particles available commercially). Some  $\beta$  phase is also detected, but in much smaller proportions than in the Wp NPs batch. As TEM determined that  $WO_3$  is dominantly amorphous in the W1 NPs batch, it is expected to be

barely detectable using XRD, except through an extremely wide and faint bump around the  $25^\circ 2\theta$  value.

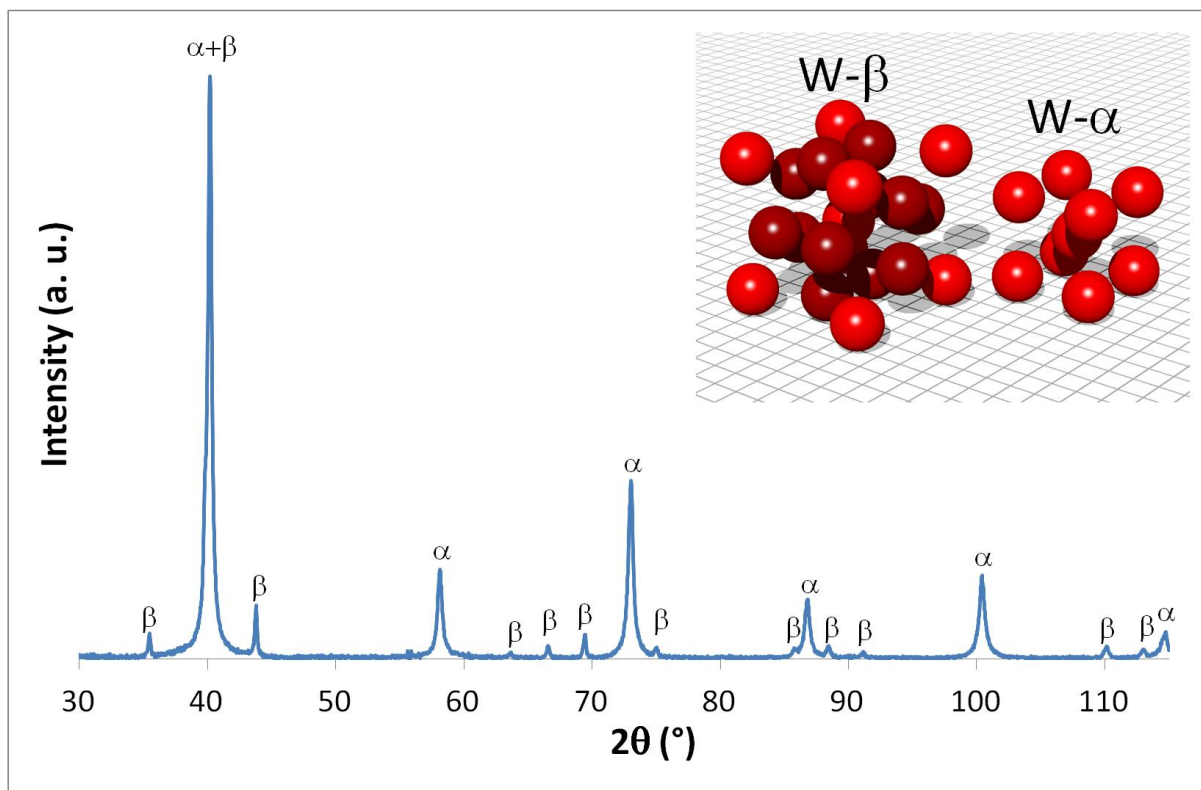


*Fig.7: XRD pattern of the W1 NPs, showing a dominant W- $\alpha$  BCC crystal structure.*

*Inset: the 2 tungsten crystal structures, with a grid size of 1Å.*

XPS measurements have been performed to check the chemical composition of the sample at the near surface area (Fig.8): XPS analysis attested to the presence of W metal in the W1 NPs batch, and confirmed that  $\text{WO}_3$  ( $\text{W}^{6+}$ ) is the major contribution among other forms previously observed for W oxidation [20]. One reasonable explanation would be that denser particles (such as droplets) contain metallic W while aggregated particles are oxides only. However XPS is mainly sensitive to particle surface and may failed in the quantification of the different W redox states from the core to the surface of W1 particles.

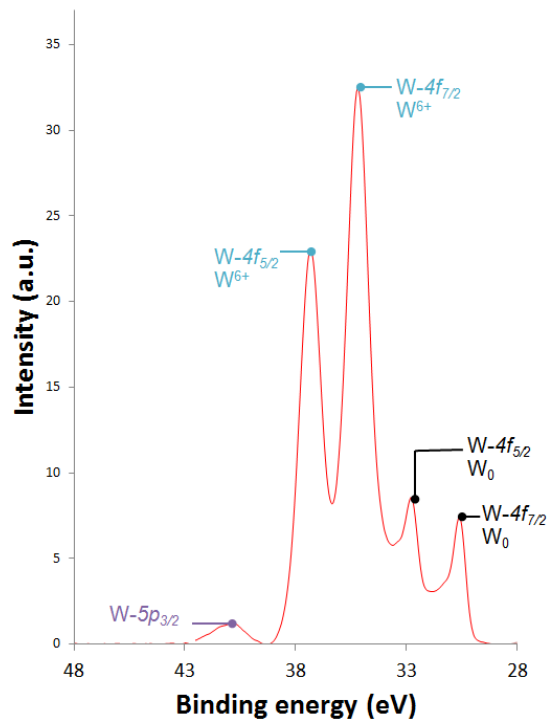


Fig.8: XPS W-4f core levels spectrum of the W1 NPs batch shows that W metal (peaks marked  $W_0$ ) is present in the sample, but the major chemical specie found in the analysed volume is  $WO_3$  oxide (peaks marked  $W^{6+}$ ).

BET analysis evaluated the SSA at  $43.5 \text{ m}^2/\text{g}$ , *i.e.* one order of magnitude higher than for Wp NPs; this was qualitatively expected from experimental observations and handling. The change in density measured by helium pycnometer was also drastic at  $8.27 \text{ g}\cdot\text{cm}^{-3}$ . A rough estimation for the W1 NPs batch composition can be made considering 70 nm diameter particles with a 19 nm  $WO_3$  outer shell, with  $W_\alpha$  phase density at  $19.262 \text{ g}\cdot\text{cm}^{-3}$ . This simple calculation gives  $WO_3$  by far the main constituent of W1 NPs, with only 5 vol. % metallic W (for the massive droplet particles) and 95 vol.%  $WO_3$ , *i.e.* 22 wt.% metallic W and 78 wt.%  $WO_3$ . This measurement confirms the tendency evaluated by the XPS analysis. X-ray absorption analysis of the sample at the W LIII edge of the W1 NPs (Fig. 4.A, black solid curve at the bottom captioned “W\_laser”), enables to determine the various redox state of W from the core to the surface. It confirmed the low proportion of metallic tungsten (Fig.4.B, solid black curves “W\_plasma” compared to the solid black curve “W\_metal (alpha)” for the



metal signature and the two dotted curves “WO<sub>2</sub>” and “WO<sub>3</sub>” for the oxides signature) in the same order of magnitude: after atomic concentration conversion to mass fraction, XAS quantification leads to 18±15% W, 32±15% WO<sub>2</sub> and 50±15% WO<sub>3</sub>. Such high oxide contents were not expected in a relatively oxygen-free production setup, even if our high vacuum system still very likely presents traces of oxygen; our hypothesis is that oxidation occurs rapidly at the (very large) surface of the particles once they are exposed to air (during their collection and storage). More studies are needed to investigate this point.

## 5. Discussion and conclusion

The similar characterization routine performed on the two samples for our study allows a global overview on the respective properties for each batch of W NPs:

- Plasma (Wp) NPs are very uniform, composed in majority of an interesting but relatively rare phase of tungsten metal; tungsten oxide is present only as a native surface layer likely due to air exposure; the specific surface area is rather low.
- Laser (Wl) NPs consists of two different populations, the dominant contribution being aggregated nano-particles mainly composed of tungsten oxide; this batch has a high specific surface area.

It is interesting to note that Wp and Wl NPs exhibit very different characteristics , while both being produced through mechanisms plausible at the plasma-wall interface in tokamaks e.g. accretion of ablated material (contrary to commercially available grinded particles). In particular, two parameters present huge disparities between the two batches: the oxide content and the specific surface area of the particles. Yet, those two parameters are crucial in the gas loading process that is used to charge the particles with tritium: on one hand, the specific surface triggers the interaction between the particle and the tritium gas atmosphere. Indeed, an increase by a factor 10 could greatly change the dynamic of the tritium absorption and

consequently the tritium trapping/desorption in W1 NPs compared to Wp NPs. On the other hand, previous studies and simulations [21] have shown that the density of traps for hydrogen is much higher in tungsten oxide than in tungsten metal. With the perspective of the tritium loading study and more generally tritiated particle behaviour studies, and in the current context of uncertainty on the characteristics of ITER-like dust, it is therefore of prime interest to consider such two different NPs samples in order to determine if drastic change in their characteristics have an impact or not. This is of course also true for biology experiments, as tritium inventory in W NPs will possibly impact toxicity for lung cells.

The next step of our study involves hydrogen isotopes (H and T) gas loading of the particles in order to estimate their potential radioactive inventory and consequences for cell toxicity. In order to distinguish respective impacts of oxide content and high SSA of H trapping in the W1 NPs, reference measurements on massive W samples were led (providing a low SSA sample with and without oxide present at the surface). The results obtained will be presented in another paper [22].

In this paper we have exemplified important physicochemical variations between two types of W-NPs in dry form. Biology exposures of human cells and tissues require the suspension of the particles in various liquid media; a characterization of the chemical properties of Wp and W1 NPs in solution is therefore the first step of the toxicity study [23]. Particles properties, both dry and suspended, could be responsible for different biological effects on cells, and more particularly on lung cells which will be the most probably affected ones in case of inhalation. The size, shape or aggregation states are currently accepted as parameters which will influence the toxicological impact of manufactured nanoparticles. In this way, and for risk assessment of ITER workers, we want to underline the necessity to evaluate the toxicity of these two characterized NPs on a relevant in vitro lung model [24].

## **Acknowledgments**

This work has been carried out thanks to the support of the A\*MIDEX project (n° ANR-11-IDEX-0001-02) funded by the “Investissements d’Avenir” French Government program, managed by the French research Agency (ANR). We acknowledge support from the Toxicology Program of the French Alternative Energies and Atomic Energy Commission (CEA) through the TWEET project. The authors acknowledge the European Synchrotron Radiation Facility for provision of synchrotron radiation beamtime and especially the scientists in charge of the FAME (BM30b) beamline financially supported by CNRS and CEA.

## **References**

- [1] R.A. Pitts et al., *Journal of Nuclear Materials* S48 (2013) 438.
- [2] M. Balden et al, *Nucl. Fusion* 54 (2014) 073010.
- [3] M. De Angelis et al, *Journal of Nuclear Materials* 463 (2015) 847.
- [4] C. Arnas et al., *Nuclear Materials and Energy* 11 (2017) 12-19.
- [5] E. Fortuna-Zalesna et al., *Nuclear Materials and Energy* 12 (2017) 582-587.
- [6] M. Shimada et al., *Journal of Nuclear Materials* 438 (2013) S996–S1000.
- [7] J. Vendel et al., *Journal of Physics: Conference Series* 170 (2009) 012026.
- [8] C.N. Davies, *Air filtration*, Academic press (1973) New York.
- [9] S.L. Alderman et al., *Journal of Occupational and Environmental Hygiene* 5: 11 (2008) 713-720.
- [10] N. Endstrasser et al., *Physica Scripta* T145 (2011) 014021.
- [11] A. Rondeau et al., *Journal of Nuclear Materials* 463 (2015) 873-876.
- [12] L. Couëdel et al., *Physics of Plasmas* 21 (2014) 123703.
- [13] K. Ouaras et al., *Journal of Physics D: Applied Physics* 51 (2018) 105303.

- [14] T. Acsente et al., The European Physical Journal D 69 (2015) 69.
- [15] A. Vatry et al., Applied Surface Science 225 (2009) 5569.
- [16] S. Brunauer et al., Journal of the American Chemical Society 60 (2) (1938) 309.
- [17] H.A. Wriedt, Journal of Phase Equilibria, 10 (1989) 368.
- [18] P. A. O'Day et al., Am. Mineral. 89 (2004) 572.
- [19] E. Bernard et al., Physica Scripta T167 (2016) 014071.
- [20] A. El-Kharbachi et al., International Journal of Hydrogen Energy 39 (2014) 10525.
- [21] X.-S. Kong et al., Journal of Nuclear Materials 433 (2013) 357.
- [22] E. Bernard et al., *Design of model tokamak particles for future toxicity studies: tritium trapping and desorption in W nano particles*, to be published.
- [23] J. Rose et al., accepted for publication in Corrosion Science (2019).
- [24] I. George et al., Toxicology Letters 238 (2015) S179.